

Understanding the Crucial Significance of the Temperature and Potential Window on the Stability of Carbon Supported Pt-alloy Nanoparticles as Oxygen Reduction Reaction Electrocatalysts

Tina Đukić^{a,†}, Leonard Moriau^{a,†}, Luka Pavko^{a,b}, Mitja Kostelec^{a,b}, Martin Prokop^c, Francisco Ruiz-Zepeda^a, Martin Šala^d, Goran Dražić^a, Matija Gatalo^{a,e*}, Nejc Hodnik^{a*}

^a Department of Materials Chemistry, National Institute of Chemistry, Hajdrihova 19, 1001 Ljubljana, Slovenia

^b Faculty of Chemistry and Chemical Technology, University of Ljubljana, Večna pot 113, 1000 Ljubljana, Slovenia

^c University of Chemistry and Technology Prague, Technická 5, 166 28 Prague 6 – Dejvice, Czech Republic

^d Department of Analytical Chemistry, National Institute of Chemistry, Hajdrihova 19, 1001 Ljubljana, Slovenia

^e ReCatalyst d.o.o., Hajdrihova 19, 1001 Ljubljana, Slovenia

Keywords: Oxygen reduction reaction (ORR), intermetallic (ordered) platinum alloys, stability, temperature, potential window, redeposition, electrochemical flow cell (EFC), inductively coupled plasma mass spectrometry (ICP-MS).

[†] these authors contributed equally to this work

* to whom correspondence should be addressed: matija.gatalo@ki.si, nejc.hodnik@ki.si

ABSTRACT

The present research provides a comprehensive study of carbon-supported intermetallic Pt-alloy electrocatalysts and assesses their stability against metal dissolution in relation to the operating temperature and the potential window using two advanced electrochemical methodologies: (i) the in-house designed high-temperature disk electrode (HT-DE) methodology as well as (ii) a modification of the electrochemical flow cell coupled to an inductively coupled plasma mass spectrometer (EFC-ICP-MS), allowing for highly sensitive time- and potential-resolved measurements of metal dissolution. The findings contradict the generally accepted hypothesis that in contrast to the rate of carbon corrosion, which follows the Arrhenius law and increases exponentially with temperature, the kinetics of Pt and subsequently the less noble metal dissolution are supposed to be for the most part unaffected by temperature. On the contrary, clear evidence is presented that in addition to the importance of the voltage/potential window, the temperature is one of the most critical parameters governing the stability of Pt and thus, in the case of Pt-alloy electrocatalysts also the ability of the nanoparticles (NPs) to retain the less noble metal. Lastly, but also very importantly, results indicate that the rate of Pt redeposition significantly increases with temperature, which has been the main reason why mechanistic interpretation of the temperature-dependent kinetics related to the stability of Pt remained highly speculative until now.

INTRODUCTION

In humanity's goal to become a carbon-neutral society, mass adoption of hydrogen as the energy carrier and proton exchange membrane fuel cells (PEMFCs) as the energy production technology are becoming recognized as one of the most important pieces of the puzzle in the fight against the negative impacts of climate change.¹⁻³ In PEMFCs, hydrogen as a fuel and oxygen from the air are converted into clean electricity with water as the only by-product. This makes PEMFCs especially suitable for competing with and eventually replacing conventional internal combustion engines (ICEs) in transport related applications. Specifically, while PEMFCs are expected to find their use also in the passenger light-duty vehicles (LDVs), it is becoming increasingly more evident that they can be significantly more competitive for the use in heavier transport-related applications that require longer travel times. Thus, one of the most promising development directions that is starting to receive significant attention is, for instance, the use of PEMFCs in heavy-duty vehicles (HDVs).⁴

However, in comparison to the ICEs, the costs related to the PEMFC technology are still too high. While the cost of most of the parts of the PEMFC will benefit highly from the

economies of scale, the costs related to the precious metals, primarily Pt found in the electrocatalyst will not and might even increase at higher PEMFC market penetration.⁵ Most of the Pt is required for enhancing the kinetics of sluggish oxygen reduction reaction (ORR) on the cathode side of the PEMFC. As of today, the only electrocatalyst system to already reach the production phase is comprised of pure Pt nanoparticles (NPs) supported on partly-graphitized high-surface area carbons (Pt/C).⁶ However, according to the existing evidence,⁷ mass commercialization of PEMFC technology will not be possible without bringing the Pt amount per vehicle down to the levels comparable with the ICE vehicles. Consequently, significant efforts in the past decades have also gone towards the next electrocatalyst system projected to reach the production phase – the so-called de-alloyed Pt-alloys with other less expensive and less noble 3d transition metals such as Co, Ni or Cu.⁶ Cost reduction using Pt-alloys is possible due to two key features: (i) Pt-alloys dilute Pt-atoms inside the NPs core and thus improve Pt overall utilisation^{8–11} and (ii) they promote a higher kinetic activity towards the ORR due to a combination of a ligand, strain, coordination number and/or surface disorder effects.^{12–18}

However, while the activity benefit of Pt-alloys has become rather clear, their commercialization is currently hindered by the lack of understanding of their stability behavior. While electrocatalyst stability is of general importance, its significance becomes even more decisive for their application in HDVs – resulting from in-average longer travel distances in comparison to passenger LDVs and thus, significantly higher system lifetime requirements.⁴ Because the degradation of Pt-alloy electrocatalysts is caused by various extremely complicated phenomena,¹⁹ significant efforts have to be invested into clarifying and understanding individual mechanisms. There are two basic groups of degradation mechanisms: i) electrochemically-induced (transient) dissolution of Pt, which is closely related with the dynamics of formation/reduction of the Pt-oxide²⁰, resulting in Ostwald ripening²¹ and/or formation of metallic Pt bands in the membrane²²; ii) electrochemical and chemical carbon support corrosion²³, leading to the agglomeration²⁴ and/or detachment¹⁹ of Pt NPs. In the case of Pt-alloy NPs, one also has to deal with the dissolution of the less noble metal dissolution.^{25,26} Last but not least, closely connected to the dissolution of Pt and Ostwald ripening, general understanding of Pt redeposition phenomena in the catalyst layer is also of utmost importance.^{27–29} However, perhaps equally important as improving the intrinsic durability of an electrocatalyst is also understanding how the mentioned degradation mechanisms relate to the different operating conditions in a PEMFC.²⁴

For instance, because PEMFCs usually operate at elevated temperatures (60-80 °C¹), it is highly beneficial to understand the stability behavior of carbon-supported Pt-based electrocatalysts also in terms of the operating temperature. Rare but highly important previous studies focused mainly on the effects of temperature on the kinetics of carbon support corrosion demonstrated that higher rates of carbon oxidation are expected with increasing operating temperature of the PEMFC.^{24,30,31} On the other hand, there also exists a limited number of past studies that address the relation of Pt dissolution and temperature both on Pt NPs^{32,33} as well as bulk Pt.³⁴⁻³⁶ In addition to these studies, Cherevko and co-workers³⁷ followed with the first study on the temperature dependent dissolution of polycrystalline Pt by coupling of the scanning flow cell (SFC) with an inductively-coupled plasma mass spectrometer (ICP-MS). SFC-ICP-MS along with other recently used similar methodologies^{25,26,29,38-42} enables insights into the time-and-potential resolved dissolution of metals, providing yet another dimension to the observed electrochemical signal. Specifically to the above-mentioned work by Cherevko and co-workers³⁷, the authors reported a rather significant influence of temperature on the on-sets of both the Pt-oxide formation as well as the reduction. In other words, with an increasing temperature, the on-sets of the Pt-oxide formation during the anodic scan on the cyclic voltammogram (CV) shifted to a higher potential, whereas the on-set of the Pt-oxide reduction also shifted towards a higher potentials. On the other hand, the differences in the collected time-and-potential resolved Pt dissolution data in relation to the temperature seemed rather insignificant. With increasing temperature, they observed only a slight increase in the anodic dissolution of Pt, while perhaps even more surprisingly they observed even a decrease in the cathodic dissolution of Pt. In other words, in the work by Cherevko and co-workers³⁷ the total amount of dissolved Pt seemed to be almost constant, whereas a prior study by Jerkiewicz and co-workers concluded that the total dissolved amount of Pt with increasing temperature might be even slightly lower.³⁴ While this indicates the possibility that Pt might be stabilized with increasing temperature, Cherevko and co-workers also stated the mechanistic interpretation of the temperature-dependent kinetics remains highly speculative.³⁷ In addition to that, they have provided the idea that perhaps the decrease in the cathodic dissolution of Pt with higher temperature could be a result of an increased rate of Pt redeposition.²⁷⁻²⁹ With no follow-up studies further addressing the mechanistic interpretation of temperature dependence of Pt dissolution, many open questions remained. For instance, does the rate of Pt redeposition increase or decrease with an increasing operating temperature? Also, how does the relation between Pt dissolution and operating temperature impact the dissolution of the less noble metal in the case of Pt-alloys? In addition to these questions, another potentially unresolved

conception in the fuel cell community is also whether the growth of the Pt NPs observed at the elevated temperatures is due to carbon support corrosion and successive Pt agglomeration or due to Pt Ostwald ripening?⁴³ Most reports explain their results by the logical notion that corrosion of carbon support becomes massive at temperatures approaching real fuel cell conditions.^{44,45} On the other hand, other studies once again also suggest Pt redeposition.³⁰ While it is far from trivial to answer all of these questions, additional complexity can be introduced when one considers also the importance of the operating voltage/potential. There are a few (but very important) examples in the literature that provide evidence that both the upper voltage/potential limit (UVL/UPL), as well as the lower voltage/potential limit (LVL/LPL) are important for limiting the degradation of Pt-based carbon supported electrocatalysts in the PEMFC. For example, Uchimura and co-workers⁴⁶ provided evidence of increasing electrochemically active surface area (ECSA) losses upon performing 15 000 accelerated degradation test (ADT) cycles under H₂-N₂ feed (Anode/Cathode, respectively) at 80 °C and 100% RH in 25 cm² fuel cells using a fixed UVL of 0.95 V while gradually lowering the LVL from 0.8 V towards the 0.6 V. The authors have attributed this to increased Pt dissolution resulting from anodic Pt-oxide formation followed by only some cathodic Pt-dissolution due to de-stabilization of the previously formed oxide species. Years later, the transient nature of Pt-dissolution was experimentally demonstrated by Topalov and co-workers with SFC-ICP-MS.⁴⁷ As a part of the Toyota Mirai launch in 2015, Yoshida and co-workers⁴⁸ affirmed the necessity of limiting both the UVL and the LVL in order to minimize the ECSA losses during fuel cell operation. Further revelations followed with the Department of Energy (DoE) Mirai Fuel Cell Vehicle report that has shown system-level limitations on the LVL of the Mirai fuel cell stack.⁴⁹ Last but not least, while avoiding high UVLs as a consequence of start-up/shut-down conditions is important mostly for avoiding severe carbon corrosion,⁵⁰ our recent work shows that especially for Pt-alloy cathodes, the choice of LVL/LPL plays a decisive role in extending the PEMFC lifetime. Namely, a profound difference in voltage degradation at 1.5 A cm⁻² in a 50 cm² single-cell has been observed during only a thousand ADT cycles (1000 cycles, 0.925-0.X V_{RHE}; X=70/60/50, 3 second hold at both LVL and UVL; ambient outlet pressures, stoichiometry 1.5/2, dew point 50 °C anode and cathode; H₂/N₂) in the case where the LVL was lowered from 0.7 to 0.6 or even 0.5 V. Interestingly, for all three LVL, the rate of voltage degradation increased with increasing operating temperature during the ADT. In addition, as part of the same work, the degradation effect has also been observed with the electrochemical flow cell coupled (EFC) to an ICP-MS. What we have noticed is that with decreasing LPL (from 0.7 to 0.65 to 0.6 V), an increase in cathodic dissolution of Pt

occurs. This was directly followed by an increase in the cathodic dissolution of the less noble metal. Thus, we have concluded that the dissolution of the less noble metal is closely connected with the dynamics of the Pt-oxide formation and reduction. UVL/UPL corresponds to the amount of anodically formed Pt-oxide, which is then followed by now already well-known oxide-place exchange mechanism^{47,51} that results in cathodic dissolution of Pt. In the case of Pt-alloys, cathodic and anodic dissolution of Pt is then always followed by also dissolution of the less noble metal.^{25,26} The rate of this process is then defined by the UVL/UPL – the lower we go, the more Pt-oxide we reduce, subsequently triggering a higher degree of metal dissolution. While this might not be of a particular importance for pure-Pt cathodes, aging of the Pt-alloy cathode will not only result in the decrease in kinetic performance, but also additional degradation phenomenon related with the presence of the less noble metal ions in the catalyst layer and/or the membrane.^{52,53}

The present research provides a comprehensive study of carbon-supported intermetallic Pt-alloy electrocatalysts and assesses their stability against metal dissolution in relation to the operating temperature and the potential window using two advanced electrochemical methodologies. For the stability assessment, proprietary intermetallic Pt-M catalysts from ReCatalyst d.o.o. were developed based on the work published elsewhere.^{31,54} In the first part, a study is conducted using our previously reported and in-house designed high-temperature disc electrode setup (HT-DE).²⁴ HT-DE setup enables one to perform ADTs at various elevated temperatures by using a reflux cooling condenser in order to avoid evaporation of the electrolyte (in our case 0.1 M HClO₄). Furthermore, specific activity (SA), mass activity (MA) and electrochemically active surface area normalized *via* CO-electrooxidation (ESCA_{CO}) before and after the ADT are evaluated using a typical thin-film rotating disc electrode setup (TF-RDE). In addition to the electrochemical evaluation of the electrocatalyst, one can also determine the amount of dissolved less noble metal by sampling the electrolyte after the ADT using ICP-OES. In order to further complement the findings of the HT-DE study and obtain mechanistic insights, already well-established^{26,28,29,38,40,41,55} highly sensitive (ppb range) electrochemical flow cell coupled to an inductively coupled plasma mass spectrometer (EFC-ICP-MS) methodology is used in the second part of this work to enable time-and-potential resolved measurements of metal dissolution. The latter has been for the purpose of the study additionally upgraded to enable investigation of metal dissolution at various temperatures (**Scheme 1**; hereinafter referred to as HT-EFC-ICP-MS).

EXPERIMENTAL

Synthesis of the intermetallic d-int-Pt-M/C electrocatalysts.

The ReCatalyst electrocatalysts were prepared in accordance with the processes already reported previously.^{31,56} Briefly, the electrocatalysts have been prepared in three steps. In the first step, Pt NPs were deposited onto a commercial carbon black support (Ketjen Black EC300J) *via* double passivation galvanic displacement method reported elsewhere.³¹ In the second step, the prepared composites with deposited Pt NPs were thermally annealed in order to obtain an intermetallic crystal phase. In the last step de-alloying (acid washing) was performed in accordance to the work described previously.^{57–59}

XRD analysis.

The powder X-ray diffraction (XRD) measurements of samples containing Co were carried out on a PANalytical X'Pert PRO diffractometer with Cu K α radiation ($\lambda = 1.541874 \text{ \AA}$) in the 2θ range from 10° to 60° with the 0.039° step per 300 s using full opened Pixcel detector. Samples were prepared on zero-background Si holder.

The powder X-ray diffraction (XRD) measurements of samples containing Ni and Cu were carried out on a PANalytical X'Pert PRO MPD diffractometer with Cu K α 1 radiation ($\lambda = 1.5406 \text{ \AA}$) in the 2θ range from 10° to 60° with the 0.034° step per 100 s using full opened X'Celerator detector. Samples were prepared on zero-background Si holder.

Transmission Electron Microscopy (TEM) analysis (NIC)

STEM imaging was carried out in a probe Cs-corrected scanning transmission electron microscope Jeol ARM 200 CF operated at 80 kV.

ICP-OES and digestion procedure for metal loading determination in the electrocatalyst powders.

All reagents used were of analytical grade or better. For sample dilution and preparation of standards, ultrapure water ($18.2 \text{ M}\Omega \text{ cm}^{-1}$, Milli-Q, Millipore) and ultrapure acids (HNO_3 and HCl , Merck-Suprapur) were used. Standards were prepared in-house by dilution of certified, traceable, inductively coupled plasma (ICP)-grade single-element standards (Merck CertiPUR). A Varian 715-ES ICP optical emission spectrometer was used. Prior to ICP-OES analysis, each electrocatalyst was weighted (approximately 10 mg) and digested using a microwave-assisted digestion system (Milestone, Ethos 1) in a solution of 6 mL HCl (conc.) and 2 mL HNO_3 (conc.). Samples were then filtered, and the filter paper was again submitted

to the same digestion protocol. These two times digested samples were cooled to RT and then diluted with 2 %v/v HNO₃ until the concentration was within the desired concentration range.

Accelerated degradation tests using the high-temperature disk-electrode methodology (HT-DE).

High Temperature Disk Electrode (HT-DE) setup – The accelerated degradation tests (ADTs) were performed in a setup already described as a part of our previous work (see also **SI, Figure S1**).²⁴ Briefly, the setup is comprised of a two-compartment HT-cell using 0.1 M HClO₄ electrolyte (Carl Roth, Rotipuran® Supra) with a conventional three-electrode system controlled by a potentiostat (CompactStat, Ivium Technologies). Reversible hydrogen electrode (HydroFlex®) was used as a reference (separated from the working electrode in a different compartment via a salt-bridge) and a graphite rod was used as a counter electrode (with respect to the temperature at which ADTs were performed, fresh graphite rod was used for each measurement).

Thin-film rotating disk electrode (TF-RDE) setup – While the ADTs were performed in the HT-DE setup, oxygen reduction reaction (ORR) polarisation curves and CO-electrooxidation CVs both before as well as after the ADT were measured in a typical TF-RDE setup also in accordance to our previous work.²⁴ The electrochemical measurements were conducted with a CompactStat (Ivium Technologies) in a two-compartment electrochemical cell in a 0.1 M HClO₄ electrolyte with a conventional three-electrode system. Similarly, a reversible hydrogen electrode (HydroFlex®) was used as a reference and a graphite rod as a counter electrode (again, with respect to the temperature at which ADTs were performed, a fresh graphite rod was used for each measurement).

Preparation of the thin films and the setups – The extensive cleaning was performed in order to eliminate any organic and inorganic impurity contributions that could potentially affect the stability of the studied electrocatalysts. Prior to the set of degradation experiments, all the glassware was soaked in both a base bath (mixture of KOH and isopropanol) and an acid bath (mixture of conc. HNO₃ and H₂SO₄) as well as boiled in distilled water 3 times. Prior to each experiment, the HT-cell was heated for 2 hours at 90 °C in 0.1 M HClO₄, then boiled in Milli-Q water for 2 hours, whereas the RT-cell was boiled in distilled water for 1 hour.

The working electrode was a glassy carbon (GC) disk embedded in Teflon (Pine Instruments) with a geometric surface area of 0.196 cm². The GC electrode was polished to a mirror finish with Al₂O₃ paste (particle size 0.05 µm, Buehler) on a polishing cloth (Buehler). After

polishing, the electrode was rinsed and ultrasonicated (Ultrasound bath Iskra Sonis 4) in Milli-Q/isopropanol mixture several times for 5 min. Once the GC electrode is prepared, 20 μL of 1 mg mL^{-1} fresh prepared water-based well-dispersed electrocatalyst ink was pipetted on the electrode completely covering it and dried under ambient conditions. After the drop had dried, 5 μL of Nafion solution (ElectroChem, 5 % aqueous solution) diluted in isopropanol (1:50) was added. The electrode was then mounted on the rotator (Pine Instruments).

Electrochemical characterisation – The electrode was then initially placed in the TF-RDE setup in an inert gas saturated electrolyte (0.1 M HClO_4) under potential control at 0.05 V_{RHE} using a rotator (Pine technologies). All electrocatalysts were then electrochemically activated (50 cycles between 0.05 and 1.2 V_{RHE} with a scan rate of 300 mV s^{-1} under a rotation rate of 600 rpm). After the activation, the electrolyte was exchanged for a fresh one. ORR polarisation curves were measured in an oxygen saturated electrolyte with rotation at 1600 rpm in the potential window 0.05-1.0 V_{RHE} with a scan rate of 20 mV s^{-1} . At the end of ORR polarisation curve measurement, the electrolyte was purged with CO under potentiostatic mode (0.05 V_{RHE}) in order to ensure successful CO adsorption. Afterward the remaining CO in the electrolyte had been displaced and electrolyte was saturated with Ar. CO-electrooxidation was performed using the same potential window and scan rate as in ORR, but without rotation and in an Ar saturated electrolyte. Electrochemical surface area (ECSA_{CO}) was determined by integrating the charge in CO-electrooxidation (“stripping”) experiments as described in Ref. ⁶⁰. For ORR, after subtraction of background current (due to capacitive currents), kinetic parameters were calculated at 0.9 V_{RHE} . Ohmic resistance of the electrolyte was determined and compensated for as reported in Ref. ⁶¹. Afterward, the working electrode was carefully transferred to the HT-DE setup (taking care to not introduce any impurities during the transfer process) and an ADT was performed comprised of 5000 cycles at various temperatures (RT, 50 °C and 75 °C) and potential windows (X-Y V_{RHE} ; X = 0.4, 0.6 and 0.7; Y = 1.2, 1.0, 0.925; 5000 cycles, 1 V s^{-1} , 0.1 M HClO_4). Afterward, the working electrode was again carefully transferred back to the standard TF-RDE setup and ORR polarization curve as well as CO-electrooxidation were measured once again (again at RT). In addition, after each ADT, the electrolyte from the HT-cell was sampled (in 15 mL vial) for *ex-situ* determination of Co using ICP-MS.

Ex-situ ICP-MS for the determination of metals in the electrolyte after ADTs – *Ex-situ* samples for determination of metal concentrations were collected after the ADTs and analysed using mass spectrometry with inductively coupled plasma. Samples were not diluted prior to measurement and measured as received. For preparation of standards, ultrapure water (Milli-

Q, Millipore) and ultrapure acid (HClO_4 ; Carl Roth, Rotipuran® Supra) were used. Standards were prepared in-house by dilution of certified, traceable, inductively coupled plasma-(ICP) grade single-element standards (Merck Certipur). An Agilent quadrupole ICP-MS instrument (Agilent 7900, Agilent Technologies, Santa Clara, CA), equipped with a MicroMist glass concentric nebuliser, and Peltier-cooled, Scott type spray chamber was used for the measurements. Each *ex-situ* electrolyte sample was measured 3 times and RSD for each measurement was determined. Typical RSD for Co was 3%, whereas the amount of dissolved Pt was too low for accurate and relevant *ex-situ* determination.

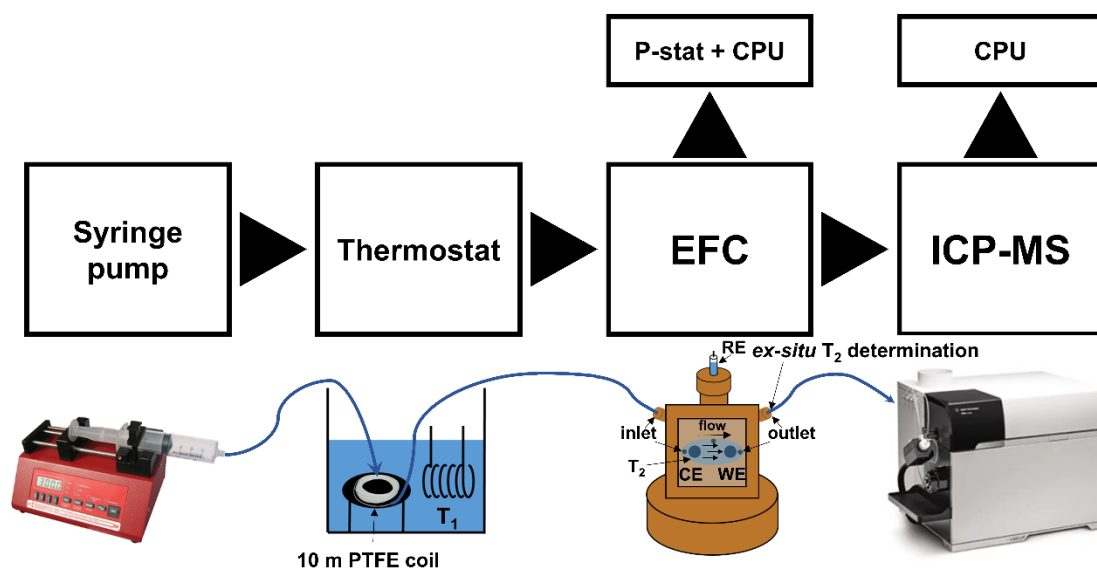
High-Temperature Electrochemical Flow Cell Coupled to Inductively Coupled Plasma Mass Spectrometry (HT-EFC-ICP-MS).

Electrochemical Flow Cell (EFC) – The setup and measurement guidelines were established as part of the previous work^{25,26,29,38–41,62}. Briefly, the working and counter electrode in the electrochemical flow cell (EFC) were glassy carbon discs (3 mm diameter) embedded into PEEK material (BASi). The discs were aligned in series; the counter electrode was placed first and the working electrode second in the direction of the electrolyte flow. The sample was deposited on the electrode by drop casting 5 μL drop of the ultrasonically homogenised catalyst ink (1 mg mL^{-1}). Such preparation resulted in the electrocatalyst loading of 5 μg for all electrocatalysts. In addition, in order to increase the surface area of the counter electrode, 5 μL drop of Ketjen Black EC300J suspension (1 mg mL^{-1}) was deposited on the glassy carbon counter electrode. After the drop had dried, 5 μL of Nafion solution (ElectroChem, 5% aqueous solution) diluted in isopropanol (1:50) was added, covering both electrodes at the same time. The Ag|AgCl reference electrode potential against RHE was determined before the start of the experiment. The housing of the cell was made from PEEK material and the design was modelled after a commercial cross-flow cell (BASi, MF-1092, cross-flow cell). The volume of the cell was established with a home-made silicon gasket with 1.0 mm thickness and 1.5 cm^2 ellipsoidal cut. The carrier solution (0.1 M HClO_4 , degassed) was first pumped through a 10 meters long PTFE tube (1/16" OD x 1.0mm ID, BGB Analytik Vertrieb GmbH) emersed in temperature-controlled (MGW Lauda thermostat) distilled water before going through the cell (**Scheme 1**; see also **SI, Figure S2**). This enabled the electrolyte (0.1 M HClO_4) sufficient time to reach the desired temperature for each experiment. Lastly, after each measurement, the actual temperature of the electrolyte was determined at the outlet of the EFC using a thermocouple (TJC1-CAXL-IM025U-150-SMP-M, Omega), whereas the path of the tubing upon exiting the water in the thermostat and the inlet of the EFC was kept constant. For the RT

measurement, the thermostat was turned off. Additionally, in order to avoid possible memory effects, each temperature (RT, 50 °C, 75 °C), as well as each measurement protocol (lower potential limit; LPL or wide potential window; WPW), were performed on a fresh catalyst film. For each temperature (RT, 50 °C, 75 °C) and potential window (LPL or WPW), each experiment was performed at least 2 times for reproducibility. The flow was kept at a constant at 400 $\mu\text{L min}^{-1}$ for all experiments using a WPI AL1000 syringe pump. The Ag|AgCl reference correction to RHE was adjusted based on the measured temperature accordingly to Ref. ³⁷.

ICP-MS – The EFC was coupled with an ICP-MS detector, namely Agilent 7900ce ICP-MS instrument (Agilent Technologies, Palo Alto, CA), equipped with a MicroMist glass concentric nebulizer and a Peltier cooled Scott-type double-pass quartz spray chamber. The signals were recorded for Cu⁶³, Ni⁶⁰, Co⁵⁹ and Pt¹⁹⁵ with 0.5 s integration per data point. To convert the ICP-MS signals to concentration (ppb), standard solution of Cu, Ni, Co and Pt in 0.1 M HClO₄ were recorded with the following concentrations: 0.5, 1, 2, 5, 10, 20, 50 and 100 ppb.

Electrochemical protocol – Electrochemical experiments were performed with a CompactStat (Ivium Technologies) with a typical three-electrode setup. No ohmic drop compensation method was used. Initially, Milli-Q water was pumped through the cell under open circuit conditions (OCP) before switching to 0.1 M HClO₄. After a steady background has been reached (for at least 2 mins), the potentiodynamic protocol was started; in order to check for the effect of the lower potential limit, the electrocatalysts were cycled for 3 cycles between 0.925-0.X V_{RHE} (X = 0.7, 0.65 and 0.6) with 9 cycles in total (scan rate of 5 mV s⁻¹). In another set of experiments, “memory effect” was checked by omitting X = 0.7 and 0.65 and only performing 3 cycles between 0.925-0.6 V_{RHE}. In both cases, the experiment was followed with two cycles between 0.05-1.4 V_{RHE} (scan rate of 5 mV s⁻¹). After each experiment, a sequence of potential pulses was performed in order to synchronise the electrochemical experiment with the ICP-MS signal.



Scheme 1: HT-EFC-ICP-MS setup used for obtaining time-and-potential resolved metal dissolution at various temperature and other ADT conditions.

RESULTS AND DISCUSSION

Figure 1 provides a comparison between the experimental d-int-Pt-Co/C electrocatalyst from ReCatalyst and a commercial Pt-Co benchmark from Umicore (Elyst Pt50 0690). High-annular dark-field TEM imaging from **Figures 1a-d** (see also **SI, Figures S3-4**) provides a general idea of the particle sizes. On the other hand, the overlap in the XRD spectra (**Figure 1e**) provides evidence that both the bulk chemical composition (Pt:Co ratio), as well as the crystal structure (intermetallic tetragonal P4/mmm crystal structure) of both, the ReCatalyst experimental electrocatalyst and the Pt-Co benchmark from Umicore are similar. The similarity of the Pt:Co chemical composition was additionally confirmed by the ICP-OES results obtained from the digestion of both electrocatalysts. In addition, while the information is not readily available directly by Umicore, the TEM analysis (see **SI, Figures S4**) along with the stability data presented later as part of this work provide strong indications that both electrocatalysts also most likely use the same carbon support (Ketjen Black EC300J). **Figures 1f-g** provide a comparison of the initial TF-RDE performance (see also **SI, Figure S5**) where ReCatalyst electrocatalyst exhibits both a higher ECSA_{CO} as well as SA than the Umicore benchmark as well as subsequently higher MA. We presume that the difference in the ECSA_{CO} can most likely be attributed to the different methods of the deposition of Pt NPs used by Umicore in contrast to ReCatalyst – the double passivation with galvanic displacement method reported previously.^{31,54} In contrast to the typically used methods, double passivation method

allows for intrinsically better dispersion by allowing for crystallization of the Pt NPs directly on the carbon support, thus combining the usually sequential nature of Pt NP synthesis and deposition steps into a single step. Thus, based on the TEM imaging from **Figures 1a-d** (see also **SI, Figures S3-4**), one could attribute this difference to the absence of the oversized (>20 nm) Pt-Co NPs in the case of ReCatalyst electrocatalyst. On the other hand, the benefit in terms of the SA, while currently unclear, could perhaps be attributed to slight differences in the thermal annealing and/or de-alloying steps.

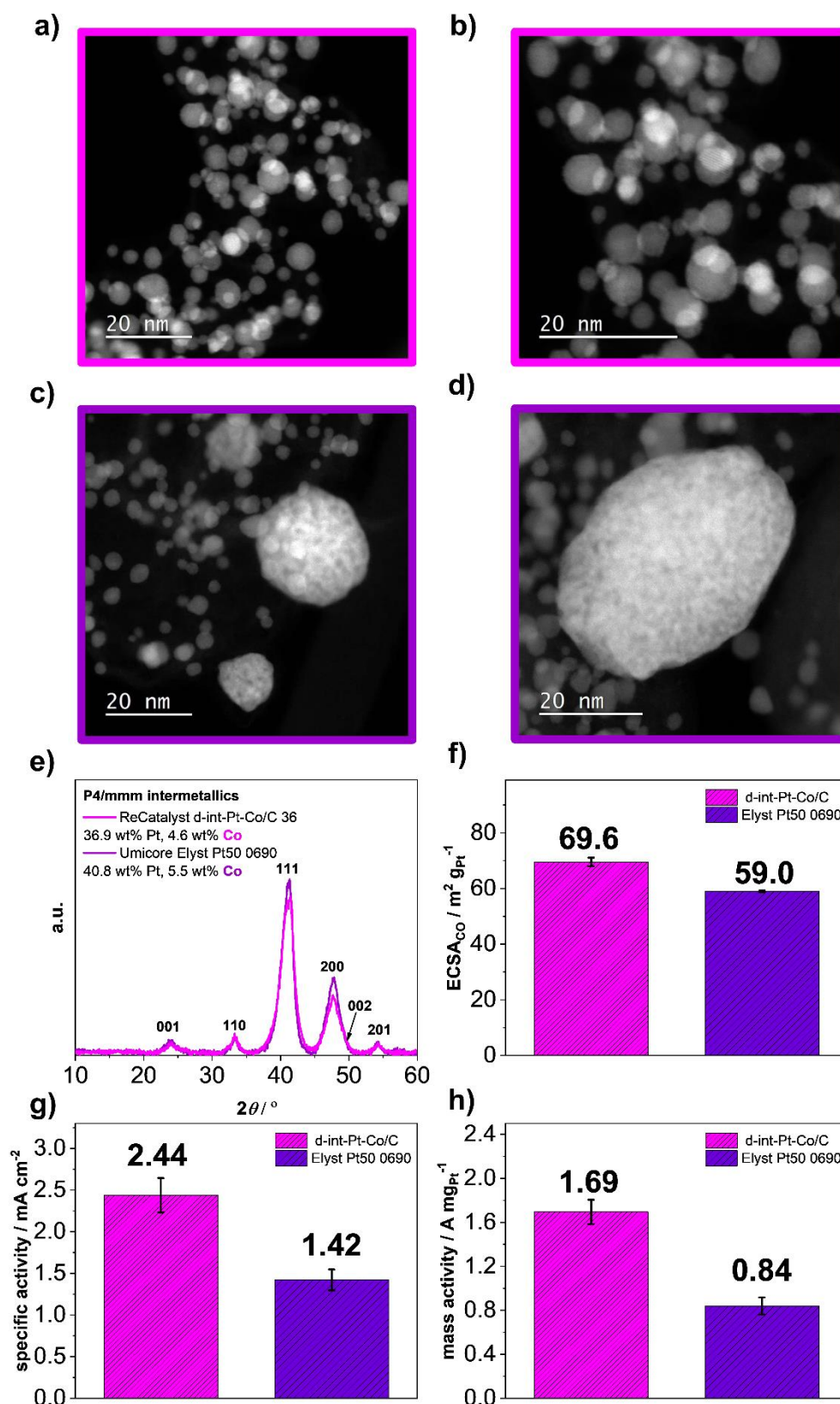


Figure 1: (a-d) HAADF TEM, (e) XRD and (f-h) TF-RDE comparison between ReCatalyst d-int-Pt-Co/C electrocatalyst and Umicore Elyst Pt50 0690 Pt-Co/C benchmark. Additional characterisation is available in the SI, Figures S3-5. In all Figures, magenta is used for the data corresponding to the experimental ReCatalyst electrocatalyst, whereas the data corresponding to the Umicore benchmark is in purple.

Prior to the interpretation of the results presented as part of the stability study, it is important to state that the main goal of this work was to investigate the stability of the ReCatalyst intermetallic Pt-Co/C electrocatalyst while obtaining the understanding related to the effects of both the temperature and the potential window. However, in the last part of the assessment, ReCatalyst electrocatalyst was additionally compared with the Umicore benchmark in order to validate that the stability of ReCatalyst electrocatalyst is indeed corresponding to the current state-of-the-art.

Figure 2 shows the assessment using the impact of the potential window (X-Y V_{RHE} ; X = 0.4, 0.6 and 0.7; Y = 1.2, 1.0, 0.925; 5000 cycles, 1 $V\ s^{-1}$, 0.1 M $HClO_4$) at a constant (elevated) temperature of 75 °C. The results are rather self-explanatory and in line with the previous studies conducted at RT.^{23,55} However, while the prior studies provide evidence in relation to the dissolution of Pt and Co in relation to the potential window, the present study using the HT-DE methodology provides information closer to the real operational conditions by performing the ADTs at 75 °C. The results indicate that narrowing of the potential window results in a lower loss of $ESCA_{Co}$, SA as well as Co. Not only that but in the case of $ESCA_{Co}$ (**Figure 2a**) and loss of Co (**Figure 2b**), a clear linear relationship is observed in the case of all measured potential windows with exception of the harshest ADT between 0.4-1.2 V_{RHE} . This is in line with the previous observations related to the transient dissolution of Pt, where in contrast to UPLs of 1.0 V or lower, an order of magnitude difference has been observed when increasing the UPL to 1.2 V_{RHE} or higher.^{20,25,26,29} While cathodic dissolution of Pt as a consequence of the place-exchange mechanism between Pt and O^{47} seems to already dominate at relatively low UPLs (as low as 0.925 V_{RHE} ⁵⁵, the results presented in **Figure 2** suggest that in the case of Pt-alloys any leaps such as the ones experienced during the start-up/shut-down conditions²³ should be avoided at all cost. In addition, as already discussed in our previous work, a significant difference is also experienced when the UPL is further reduced to 0.925 V_{RHE} and the LPL to 0.7 V_{RHE} . The main challenge that arises at this point is, however, how to avoid sacrificing a big part of the maximum power density in a single-cell setting as well as close to realistic operational conditions (air, lower humidity, etc) when the LPL is limited to 0.7 rather than 0.6 V? One way on how to partly solve this is by using higher Pt loadings at the cathode. This will in contrast to passenger LDVs (with expected cathode loadings of 0.1 $mg_{Pt}\ cm^{-2}$ or lower) suit better the application of Pt-alloys in HDVs (with expected cathode loadings of 0.25 $mg_{Pt}\ cm^{-2}$).⁴ Furthermore, heavier transport applications in general, could significantly benefit from limiting both the upper and lower voltage limits⁴⁸ and significantly increase the life as well as the long-term performance of the PEMFC stack.

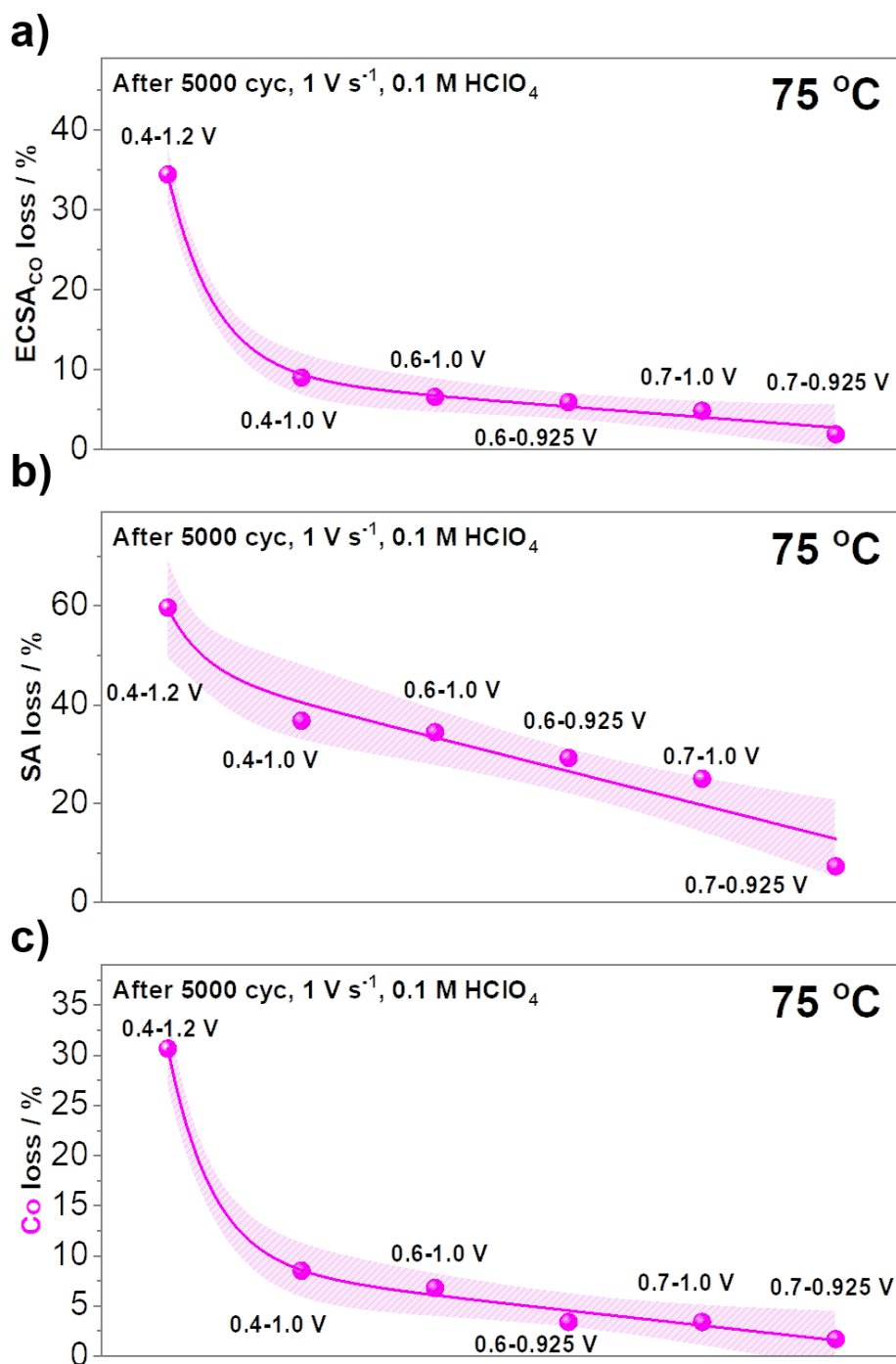


Figure 2: Effect of varying the potential window on the accelerated degradation tests (ADTs) performed at a constant temperature (75 °C, 5000 cycles, 1 V s⁻¹, 0.1 M HClO₄) comparing (a) ECSA_{Co} loss, (b) SA loss and (c) Co loss of the ReCatalyst intermetallic de-alloyed Pt-Co/C electrocatalyst. Electrochemical data can be found in SI, Figures S6-7. The experimental data in this figure was fitted only for the purpose of better visualisation.

Following the assessment of various potential windows at a constant temperature of 75 °C in **Figure 2**, we are now focusing only on the potential window that is still most typically used in the literature (several thousands of cycles between 0.6-1 V_{RHE}) and often referred to as the ‘operating conditions’.^{9,63–66} In order to demonstrate the crucial importance of the

temperature already in this potential range, we are providing a comparison between the measurement performed at the RT and the measurement performed at 75 °C (**Figure 3**). **Figures 3a-c** provide evidence that already in this relatively narrow potential window, the temperature significantly impacts the assessment of the electrocatalyst not only in the case of ESCA_{CO}, but also the SA as well as loss of Co. In addition, **Figures 3d-e** provide a comparison of CO-electrooxidation CVs as well as the follow-up cycles before and after the ADT, whereas **Figures 3f-g** compare the ORR polarization curves in the same manner. Comparison of the CO-electrooxidation shows that the overlap of the CVs before and after the ADT is much closer at RT than at 75 °C. This is in line with the comparison of the ESCA_{CO} (**Figure 3a**), where in fact the retained ESCA_{CO} after the ADT slightly increases, whereas, in the case of 75 °C, the ECSA_{CO} clearly dropped. The increase in ESCA_{CO} resulting from the ADT performed at RT can be explained that the degradation mechanisms contributing to the loss of ESCA_{CO} (*e.g.* Ostwald ripening) most likely had a lower contribution as the mechanisms that can potentially even increase it (*e.g.* formation of pores). In the case of the comparison of ORR polarization curves before and after the ADT we notice that at RT (**Figure 3f**), the polarization curves remain nicely overlapped with almost no difference observed also in the overpotential region. On the other hand, when the same ADT is performed at 75 °C (**Figure 3g**), an increase in overpotential is observed after the ADT, while the slopes of both polarization curves before and after the ADT remained similar (indicating no significant contributions from impurities). Thus, similarly to the electrocatalyst durability assessment guidelines provided as part of our previous work,²⁴ also stability evaluation of Pt-alloy electrocatalysts at the potential window of 0.6-1 V_{RHE} and RT conditions when using TF-RDE setups is less corresponding to the fuel cell operation and should in half-cell setups be performed at elevated temperatures for the correct assessment of novel electrocatalyst stability. Lastly, the higher drop in SA at 75 °C in contrast to RT (**Figures 3d & e,f**) is a consequence of an increased loss of Co (**Figure 3g**), which is in line with the loss of the beneficial ORR enhancement effects induced by Co to the Pt surface.⁶⁷

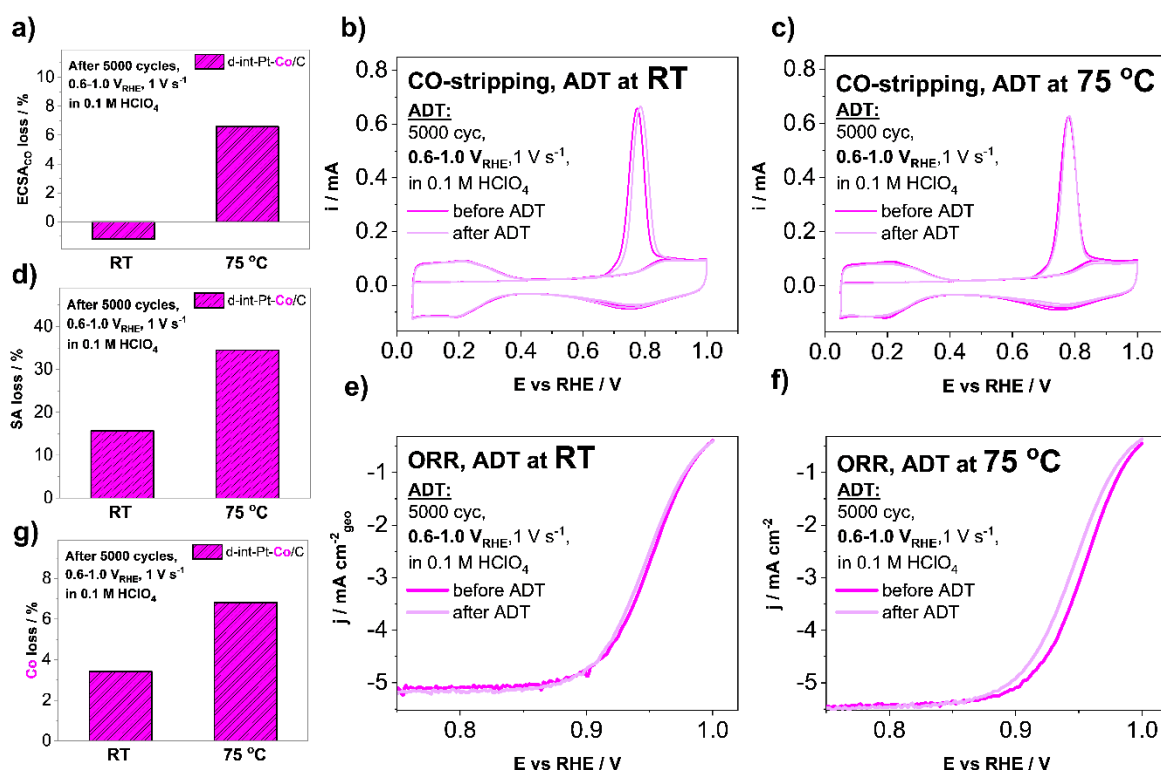


Figure 3: Effect of the temperature on the accelerated degradation tests (ADTs) performed at the potential window of 0.6-1.0 V_{RHE} (comparing RT & 75 °C, 5000 cycles, 1 $V s^{-1}$, 0.1 M $HClO_4$) comparing (a) ECSA_{CO} loss, (b) SA loss and (c) Co loss of the ReCatalyst intermetallic de-alloyed Pt-Co/C electrocatalyst. Comparison of the CO-electrooxidation CVs as well as the follow-up cycles before and after the ADT performed at (d) RT and at (e) 75 °C. Comparison of the ORR polarization curves before and after the ADT performed at (f) RT and at (g) 75 °C.

Before the evaluation of the results presented in **Figure 4** it is important to clarify clear distinctions between the prior temperature-dependent study performed by Cherevko and co-workers³⁷: (i) The prior study was performed on polycrystalline-Pt; (ii) Due to the low specific surface area of poly-Pt, all the measurements have been performed in a very wide potential window (between 0.5-1.6 or even 1.9 V_{RHE}). This is because, in addition to the low specific surface area, also the ‘bulk-like’ behavior of the poly-Pt both provide for a significantly lower signal for Pt dissolution in contrast to what can be expected in the case of Pt-based nanoparticles.²⁰; (iii) As shown in one of the recent publications by Ehelebe and co-workers²⁷, the thickness of the catalyst layer has a significant contribution to the redeposition of Pt. In other words, the thicker the catalyst layer, the longer the travel path for the dissolved Pt ions, the higher the probability for Pt redeposition. Thus, in this work, it can be expected that any Pt redeposition effects are most likely much more pronounced when dealing with electrocatalyst films comprised of composites between carbon and Pt-based NPs. Perhaps even more importantly, there is a significant benefit of not only measuring NPs rather than polycrystalline disks but also measuring Pt-alloy NPs rather than pure-Pt NPs. While more will be explained

in continuation, the main reasoning behind this is that while Pt is well-known to experience significant redeposition,^{27–29} the less noble metals with a significantly lower standard redox potential such as Co or Ni do not. Furthermore, in accordance with the evidence provided in our previous publications^{25,68} anodic and cathodic dissolution of the less noble metal are always a consequence of the anodic and cathodic dissolution of Pt.^{25,26} In other words, regardless of any Pt redeposition effects, being able to measure the dissolution of the less noble metal can be taken as an indication or a probe for what is happening with the dissolution of Pt.

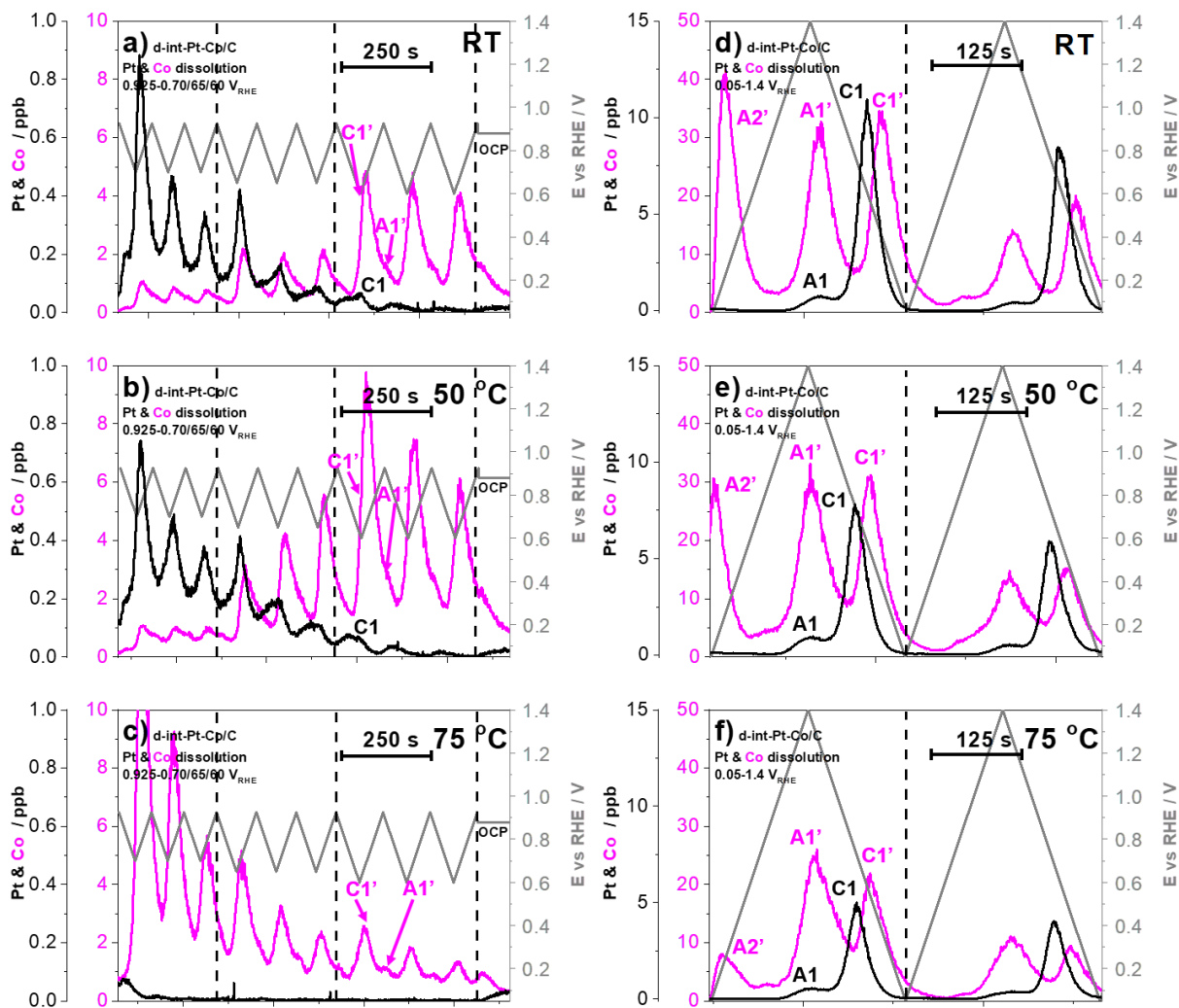


Figure 4: (a-c) Effect of temperature (RT, 50 °C, 75 °C) on the metal dissolution (Pt & Co) during the LPL cycles (0.925-0.X V_{RHE} ; X = 0.70, 0.65 and 0.60; 5 $mV s^{-1}$) and (d-f) WPW cycles (two cycles between 0.05-1.4 V_{RHE} , 10 $mV s^{-1}$) demonstrated using the HT-EFC-ICP-MS setup in the flow of 0.1 M $HClO_4$. AX and AX' represent peaks corresponding to anodic dissolution, whereas CX and CX' represent peaks corresponding to the cathodic dissolution of Pt and Co respectively. Demonstration of the same effect on the experimental intermetallic de-alloyed Pt-Cu/C and Pt-Ni/C electrocatalysts is available in the SI, Figures 8-9, whereas the methodology reproducibility example is provided in SI, Figure S10.

Figures 4a-c show the LPL effect (3 cycles each LPL, 0.925-0.X V_{RHE} ; X=70/65/60, 5 $mV s^{-1}$, 0.1 M $HClO_4$) in relation to the temperature of the electrolyte (RT, 50 °C and 75 °C).

Briefly at RT (**Figure 4a**), we notice that at a fixed UPL (in this case 0.925 V_{RHE}), upon decreasing the LPL from 0.7 to 0.65 and lastly to 0.6 V_{RHE} , an increase in the dissolution of the less noble metal (in this case Co) is observed. In general, the increase in the observed dissolution of Co in the operational potential window (0.925-0. X V_{RHE} ; X=70/65/60) is predominantly a consequence of the cathodic dissolution of Pt. By decreasing the LPL, we are reducing increasingly more Pt-oxide during the cathodic scan and thus, forming low coordinated Pt atoms that can get dissolve as a result of the oxide-place exchange mechanism.⁴⁷ Once Pt dissolves, it exposes previously protected Co atoms, thus leading to the subsequent dissolution of Co. Upon increasing the temperature of the electrolyte to 50 °C (**Figure 4b**), we notice that in comparison to the RT measurement (**Figure 4a**) the dissolution of Pt remains very similar or even slightly decreased. On the other hand, we notice that the dissolution of Co in fact almost doubled at the LPLs of 0.65 and 0.6 V_{RHE} . Before further explanation, let's look at what happens if the temperature is increased to 75 °C (**Figure 4c**). We notice that the signal corresponding to the dissolution of Pt has nearly dropped into the background. However, rather surprisingly, in contrast to the measurements performed at RT and 50 °C, the dissolution of Co is already significant at the highest LPL of 0.7 V_{RHE} . First and foremost, as mentioned previously, the dissolution of Co is an indication that there is dissolution of Pt. While we observe a lower signal for Pt with an increasing temperature, two things are actually happening: (i) in accordance to the prior work by Cherevko and co-workers,³⁷ with increasing temperature the on-set of Pt-oxide reduction is shifted towards higher potentials. In other words, this means that at the same potential window but with increasing electrolyte temperature, a higher degree of cathodically dissolved Pt resulting from the oxide-place exchange mechanism is expected. Since the dissolution of Pt and the less noble metal are connected^{25,68}, a higher degree of Pt dissolution also means more dissolved Co, which is exactly the trend we observe in **Figures 4a-c**; (ii) since we observe a decreasing trend (signal) for Pt dissolution with increasing temperature (**Figures 4a-c**), this in some way contradicts our previous statement and one could easily conclude that less Pt is being dissolved upon increasing the temperature. However, as already predicted as a possibility by Cherevko and co-workers³⁷, the observed decrease in the dissolution of Pt with increasing temperature (**Figures 4a-c**) is in fact a consequence of much more efficient redeposition of Pt. In other words, a higher amount of Pt dissolves, but at the same time also redeposits back in the relatively thick catalyst film and thus, does not reach the ICP-MS detector.

Figures 4d-f on the other hand, show the wide potential window (WPW) cycles (III.; two WPW cycles, 0.05-1.4 V_{RHE} , 10 mV s⁻¹, 0.1 M HClO₄). Here we wish to remind the reader

that each of the 6 measurements in **Figure 4** was performed on a fresh catalyst film, thus avoiding any memory effects. In contrast to the LPL experiments (**Figures 4a-c**), the WPW experiments (**Figures 4d-f**) are more easily relatable to the prior work by Cherevko and co-workers.³⁷ Similarly to their work, we, with increasing temperature, observe a decrease in the signal related to the cathodic dissolution of Pt as well as a decrease in the shift of the peak maximum towards higher potentials. This is in accordance with two already explained phenomena – (i) shift in the cathodic peak maximum of Pt due to the shift in the on-set of Pt-oxide reduction towards higher potentials and (ii) a decrease in the signal corresponding to the cathodic dissolution of Pt due to a higher degree of Pt redeposition with increasing temperature. Furthermore, in contrast to the LPL experiments (**Figures 4a-c**), we interestingly in the case of WPW experiments (**Figures 4d-f**) observe only minor differences in the dissolution of Co with increasing temperature. This is because unlike in the case of LPL experiments (**Figures 4a-c**), where only a part of Pt-oxide gets reduced upon the cathodic scan till 0.7, 0.65 or 0.6 V_{RHE}, by going as low as 0.05 V_{RHE} as in the case of WPW experiments (**Figures 4a-c**) Pt-oxide gets reduced entirely regardless of the temperature. Consequently, any differences related to Co dissolution at wide potential windows become less significant, or in other words, the effect of temperature on the stability of Pt-alloys is much more important in the case of PEMFC operational voltage window (*i.e.* 0.6-0.95 V).

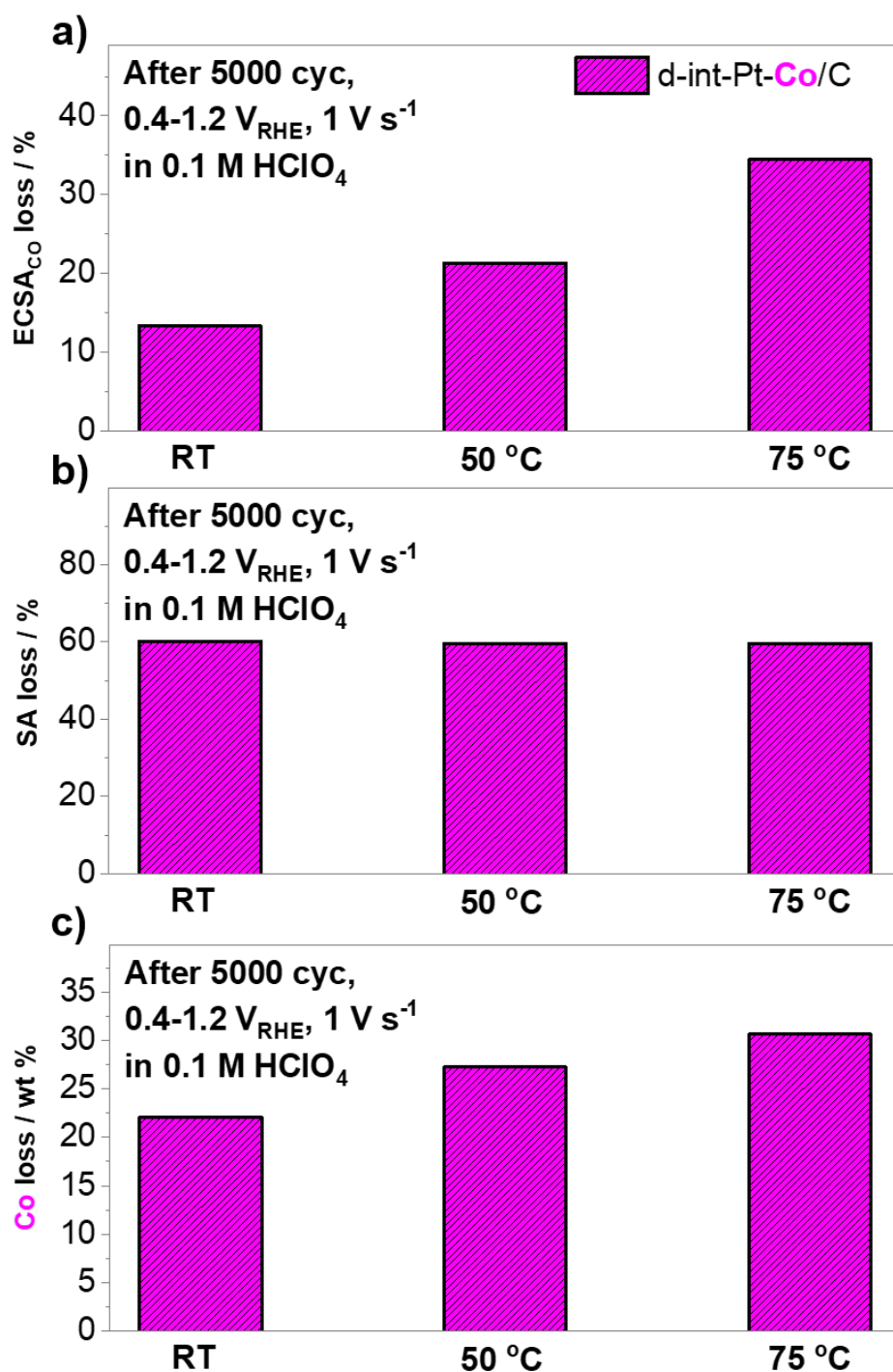


Figure 5: Effect of the temperature on the accelerated degradation tests (ADTs) performed at a constant potential window (0.4-1.2 V_{RHE}, 5000 cycles, 1 V s⁻¹, 0.1 M HClO₄) comparing (a) ECSA_{Co} loss, (b) SA loss and (c) Co loss of the ReCatalyst intermetallic de-alloyed Pt-Co/C electrocatalyst. Electrochemical data along with a comparison with Elyst Pt50 0690 benchmark from Umicore can be found in SI, Figures 11-12.

Lastly, the final assessment (Figure 5) provides for a comparison of the ReCatalyst electrocatalyst at various temperatures (RT, 50 °C and 75 °C), but at constant potential window including other ADT conditions (0.4-1.2 V_{RHE}, 5000 cycles, 1 V s⁻¹, 0.1 M HClO₄). While these conditions are unrealistic in terms of expected operational conditions of a PEMFC (0.6-0.95

V), they resemble the harsher conditions used during our previous assessment of Pt/C electrocatalysts from Tanaka Kikinzoku Kogyo used for the validation of the in-house designed HT-DE methodology in our previous work.²⁴ **Figure 5a** shows that ECSA_{CO} loss follows the expected trend of RT < 50 °C < 75 °C. Looking at the past literature, one could assume that an increase in ECSA_{CO} loss with increasing temperature is primarily a consequence of increased corrosion of the carbon support, followed by coalescence and agglomeration of Pt-based NPs.^{24,30,31} However, the results in the present study (**Figures 2-4**) provide strong evidence that the increase in metal dissolution and redeposition (Ostwald ripening) with increasing temperature perhaps holds more significant importance for the increasing ECSA_{CO} loss trend observed in **Figure 5a**. On the other hand, in contrast to the temperature comparison the case of the potential window of 0.6-1.0 V_{RHE} (**Figure 3**), in the case of the potential window of 0.4-1.2 V_{RHE}, loss in SA for ORR seems to be similar regardless of the temperature used in the ADT (**Figure 5b**). One could explain this that regardless of the temperature when performing 5000 cycles while using such an aggressive and wide potential window, the Pt-Co intermetallic NPs eventually reach the same quasi-stable state.⁶⁹ However, most likely in the case of performing the ADT at 75 °C, one reaches such a state after a significantly lower number of cycles. Lastly, **Figure 5c** compares the amount of lost Co that follows a similar trend as ECSA_{CO} – RT < 50 °C < 75 °C.

CONCLUSIONS

The findings of this study contradict the generally accepted hypothesis that in contrast to the rate of carbon corrosion that follows the Arrhenius law and increases exponentially with temperature, the kinetics of Pt and subsequently the less noble metal dissolution are supposed to be for the most part unaffected by temperature.⁷⁰ However, clear evidence is presented that in addition to the importance of the voltage/potential window,^{23,24} temperature is in fact the most critical parameter governing the stability of Pt and thus, in the case of Pt-alloy electrocatalysts also the ability of the NPs to retain the less noble metal. In addition, based on the mechanistic insights obtained with the HT-EFC-ICP-MS, the findings of this study also provide evidence that the observations by Cherevko and co-workers³⁷ on Polycrystalline Pt are indeed a consequence of severe Pt redeposition at increased temperature. This also hints that at elevated temperatures carbon supported Pt-based electrocatalysts degrade also via the Ostwald ripening mechanism and not just the carbon corrosion-induced Pt agglomeration. The results can be summarised in the following main messages:

- HT-DE methodology revealed that a higher temperature of the electrolyte in the form of 0.1 M HClO₄ will result in an increased loss of ESCA_{Co}, SA as well as an increase in the loss of Co. At the same temperature (*e.g.* 75 °C) this is also true when one expands the potential window – both the lower or the upper potential limit. While the relation seems to be rather linear for upper potential limits of 1.0 V or below, it becomes exponential if the potential is to be increased to 1.2 V (or higher).
- Evaluating the stability of novel Pt-alloy electrocatalysts at RT and in the potential window of 0.6-1 V is insufficient. This work provides evidence that performing ADTs under such a potential window at 75 °C, not only a noticeably higher loss of ESCA_{Co} and SA is observed, but also a higher amount of the less noble metal is lost. While this additional dissolved Co in the present study gets diluted in a large amount of the electrolyte, one can expect a significantly higher impact if such an amount of Co would be dissolved in a fuel cell.⁵³ In addition, further narrowing of the operational window (*e.g.* 0.7-0.925 V) results in a significant decrease in the detected amounts of dissolved Co.
- HT-EFC-ICP-MS methodology on the other hand revealed that most likely, different dynamics of Pt-oxide formation and reduction at elevated temperature conditions (shifting in the onset to positive potentials)³⁷ are responsible for the increased dissolution of Pt with increasing temperature. At the same potential window, more Pt-oxide is reduced resulting in more transiently dissolved Pt as a result of the oxide-place exchange mechanism. Nevertheless, this increase in Pt dissolution is masked by also a significant increase in the Pt redeposition in the catalyst layer. However, because less noble metal dissolution (dealloying) is a consequence of Pt dissolution,²⁶ the observed increase in the less noble metal dissolution with increasing temperature provides evidence of what is going on with Pt. Thus, a significant increase in the cathodic less noble metal dissolution already in the potential window of 0.7-0.925 V is observed with increasing temperature.

This work provides a significant contribution towards lowering of the so-far highly speculative mechanistic interpretation of the temperature and potential window-dependent kinetics of metal dissolution and the likely mechanisms behind them. In addition, the work shows significant evidence that while intermetallics of Pt are quite stable when used under rather narrow operational windows/voltages, they do not stop the leaching of the less noble metal under none of the used ADT conditions. Nevertheless, this work also provides not only the guidance to the PEMFC community on the investigation of the stability of novel Pt-alloy electrocatalysts, but also add value to the importance of designing a more stable catalyst layer

that accounts for redeposition and operating voltage as well as to the system-level producers who need to provide for the crucial hardware and/or software solutions at limiting the operating voltage as well.

Acknowledgements

The authors would like to acknowledge the Slovenian research agency (ARRS) programs P2-0393, P1-0034; the projects NC-0007; and European Research Council (ERC) Starting Grant 123STABLE (Grant agreement ID: 852208) and Proof of Concept Grant StableCat (Grant agreement ID: 966654) for funding the study.

REFERENCES

- (1) Kodama, K.; Nagai, T.; Kuwaki, A.; Jinnouchi, R.; Morimoto, Y. Challenges in Applying Highly Active Pt-Based Nanostructured Catalysts for Oxygen Reduction Reactions to Fuel Cell Vehicles. *Nat. Nanotechnol.* **2021**, *16*, 140–147.
- (2) The European Green Deal:Clean Energy.
https://ec.europa.eu/commission/presscorner/detail/en/fs_19_6723 (Date accessed: 09.Sept.2020).
- (3) Katsounaros, I.; Cherevko, S.; Zeradjanin, A. R.; Mayrhofer, K. J. J. Oxygen Electrochemistry as a Cornerstone for Sustainable Energy Conversion. *Angew. Chemie Int. Ed.* **2014**, *53*, 102–121. <https://doi.org/10.1002/anie.201306588>.
- (4) Cullen, D. A.; Neyerlin, K. C.; Ahluwalia, R. K.; Mukundan, R.; More, K. L.; Borup, R. L.; Weber, A. Z.; Myers, D. J.; Kusoglu, A. New Roads and Challenges for Fuel Cells in Heavy-Duty Transportation. *Nat. Energy* **2021**.
<https://doi.org/10.1038/s41560-021-00775-z>.
- (5) Kongkanand, A.; Mathias, M. F. The Priority and Challenge of High-Power Performance of Low-Platinum Proton-Exchange Membrane Fuel Cells. *J. Phys. Chem. Lett.* **2016**, *7* (7), 1127–1137. <https://doi.org/10.1021/acs.jpcllett.6b00216>.
- (6) Banham, D.; Ye, S. Current Status and Future Development of Catalyst Materials and Catalyst Layers for Proton Exchange Membrane Fuel Cells: An Industrial Perspective. *ACS Energy Lett.* **2017**, *2* (3), 629–638. <https://doi.org/10.1021/acsenenergylett.6b00644>.
- (7) Gittleman, C. S.; Kongkanand, A.; Masten, D.; Gu, W. Materials Research and Development Focus Areas for Low Cost Automotive Proton-Exchange Membrane Fuel Cells. *Curr. Opin. Electrochem.* **2019**, *18*, 81–89.
<https://doi.org/10.1016/J.COEELEC.2019.10.009>.
- (8) Huang, X.; Zhao, Z.; Cao, L.; Chen, Y.; Zhu, E.; Lin, Z.; Li, M.; Yan, A.; Zettl, A.;

- Wang, Y. M.; Duan, X.; Mueller, T.; Huang, Y. High-Performance Transition Metal-Doped Pt₃Ni Octahedra for Oxygen Reduction Reaction. *Science* **2015**, *348* (6240), 1230–1234. <https://doi.org/10.1126/science.aaa8765>.
- (9) Chen, C.; Kang, Y.; Huo, Z.; Zhu, Z.; Huang, W.; Xin, H. L.; Snyder, J. D.; Li, D.; Herron, J. a; Mavrikakis, M.; Chi, M.; More, K. L.; Li, Y.; Marković, N. M.; Somorjai, G. a; Yang, P.; Stamenković, V. R. Highly Crystalline Multimetallic Nanoframes with Three-Dimensional Electrocatalytic Surfaces. *Science* **2014**, *343* (6177), 1339–1343. <https://doi.org/10.1126/science.1249061>.
- (10) Choi, S.; Xie, S.; Shao, M.; Odell, J. H.; Lu, N.; Peng, H.-C.; Protsailo, L.; Guerrero, S.; Park, J.; Xia, X.; Wang, J.; Kim, M. J.; Xia, Y. Synthesis and Characterization of 9 Nm Pt–Ni Octahedra with a Record High Activity of 3.3 A/MgPt for the Oxygen Reduction Reaction. *Nano Lett.* **2013**, *13*, 3420–3425. <https://doi.org/10.1021/nl401881z>.
- (11) Stamenković, V. R.; Fowler, B.; Mun, B. S.; Wang, G.; Ross, P. N.; Lucas, C. a; Marković, N. M. Improved Oxygen Reduction Activity on Pt₃Ni(111) via Increased Surface Site Availability. *Science* **2007**, *315* (5811), 493–497. <https://doi.org/10.1126/science.1135941>.
- (12) Toda, T.; Igarashi, H.; Uchida, H.; Watanabe, M. Enhancement of the Electroreduction of Oxygen on Pt Alloys with Fe , Ni , and Co. *J. Electrochem. Soc.* **1999**, *146* (10), 3750–3756. <https://doi.org/10.1149/1.1392544>.
- (13) Stonehart, P. Development of Advanced Noble Metal-Alloy Electrocatalysts for Phosphoric Acid Fuel Cells (PAFC). *Berichte der Bunsengesellschaft für Phys. Chemie* **1990**, 913–921. <https://doi.org/10.1007/BF01029576>.
- (14) Stamenković, V.; Mun, B. S.; Mayrhofer, K. J. J.; Ross, P. N.; Marković, N. M.; Rossmeisl, J.; Greeley, J.; Nørskov, J. K. Changing the Activity of Electrocatalysts for Oxygen Reduction by Tuning the Surface Electronic Structure. *Angew. Chemie (International ed.)* **2006**, *45* (18), 2897–2901. <https://doi.org/10.1002/anie.200504386>.
- (15) Strasser, P.; Koh, S.; Anniyev, T.; Greeley, J.; More, K.; Yu, C.; Liu, Z.; Kaya, S.; Nordlund, D.; Ogasawara, H.; Toney, M. F.; Nilsson, A. Lattice-Strain Control of the Activity in Dealloyed Core-Shell Fuel Cell Catalysts. *Nat. Chem.* **2010**, *2* (April), 454–460. <https://doi.org/10.1038/nchem.623>.
- (16) Čolić, V.; Bandarenka, A. S. Pt Alloy Electrocatalysts for the Oxygen Reduction Reaction: From Model Surfaces to Nanostructured Systems. *ACS Catal.* **2016**, *6* (8), 5378–5385. <https://doi.org/10.1021/acscatal.6b00997>.

- (17) Calle-Vallejo, F.; Tymoczko, J.; Colic, V.; Vu, Q. H.; Pohl, M. D.; Morgenstern, K.; Loffreda, D.; Sautet, P.; Schuhmann, W.; Bandarenka, A. S. Finding Optimal Surface Sites on Heterogeneous Catalysts by Counting Nearest Neighbors. *Science* **2015**, *350* (6257), 185–189. <https://doi.org/10.1126/science.aab3501>.
- (18) Chattot, R.; Le Bacq, O.; Beermann, V.; Kühl, S.; Herranz, J.; Henning, S.; Kühn, L.; Asset, T.; Guétaz, L.; Renou, G.; Drnec, J.; Bordet, P.; Pasturel, A.; Eychmüller, A.; Schmidt, T. J.; Strasser, P.; Dubau, L.; Maillard, F. Surface Distortion as a Unifying Concept and Descriptor in Oxygen Reduction Reaction Electrocatalysis. *Nat. Mater.* **2018**, *17* (9), 827–833. <https://doi.org/10.1038/s41563-018-0133-2>.
- (19) Meier, J. C.; Galeano, C.; Katsounaros, I.; Witte, J.; Bongard, H. J.; Topalov, A. A.; Baldizzone, C.; Mezzavilla, S.; Schüth, F.; Mayrhofer, K. J. J. Design Criteria for Stable Pt/C Fuel Cell Catalysts. *Beilstein J. Nanotechnol.* **2014**, *5* (1), 44–67. <https://doi.org/10.3762/bjnano.5.5>.
- (20) Cherevko, S.; Kulyk, N.; Mayrhofer, K. J. J. Durability of Platinum-Based Fuel Cell Electrocatalysts: Dissolution of Bulk and Nanoscale Platinum. *Nano Energy* **2016**, *29*, 275–298. <https://doi.org/10.1016/j.nanoen.2016.03.005>.
- (21) Ahluwalia, R. K.; Arisetty, S.; Peng, J.-K.; Subbaraman, R.; Wang, X.; Kariuki, N.; Myers, D. J.; Mukundan, R.; Borup, R.; Plevaya, O. Dynamics of Particle Growth and Electrochemical Surface Area Loss Due to Platinum Dissolution. *J. Electrochem. Soc.* **2014**, *161* (3), F291–F304. <https://doi.org/10.1149/2.051403jes>.
- (22) Bi, W.; Gray, G. E.; Fuller, T. F. PEM Fuel Cell Pt/C Dissolution and Deposition in Nafion Electrolyte. *Electrochem. Solid-State Lett.* **2007**, *10* (5), B101. <https://doi.org/10.1149/1.2712796>.
- (23) Pizzutillo, E.; Geiger, S.; Grote, J.-P.; Mingers, A.; Mayrhofer, K. J. J.; Arenz, M.; Cherevko, S. On the Need of Improved Accelerated Degradation Protocols (ADPs): Examination of Platinum Dissolution and Carbon Corrosion in Half-Cell Tests. *J. Electrochem. Soc.* **2016**, *163* (14), F1510–F1514. <https://doi.org/10.1149/2.0731614jes>.
- (24) Maselj, N.; Gatalo, M.; Ruiz-Zepeda, F.; Kregar, A.; Jovanović, P.; Hodnik, N.; Gaberšček, M. The Importance of Temperature and Potential Window in Stability Evaluation of Supported Pt-Based Oxygen Reduction Reaction Electrocatalysts in Thin Film Rotating Disc Electrode Setup. *J. Electrochem. Soc.* **2020**, *167* (11), 114506. <https://doi.org/10.1149/1945-7111/aba4e6>.
- (25) Gatalo, M.; Jovanović, P.; Petek, U.; Šala, M.; Šelih, V. S.; Ruiz-Zepeda, F.; Bele, M.;

- Hodnik, N.; Gabersček, M. Comparison of Pt–Cu/C with Benchmark Pt–Co/C: Metal Dissolution and Their Surface Interactions. *ACS Appl. Energy Mater.* **2019**. <https://doi.org/10.1021/acsaem.8b02142>.
- (26) Moriau, L. J.; Hrnjić, A.; Pavlišić, A.; Kamšek, A. R.; Petek, U.; Ruiz-Zepeda, F.; Šala, M.; Pavko, L.; Šelih, V. S.; Bele, M.; Jovanovič, P.; Gatalo, M.; Hodnik, N. Resolving the Dilemma of Nanoparticles' Structure-Property Relationships at the Atomic Level: Case Study of Pt-Based Oxygen Reduction Electrocatalysts. *iScience* **2021**, 102102. <https://doi.org/10.1016/j.isci.2021.102102>.
- (27) Ehelebe, K.; Knöppel, J.; Bierling, M.; Mayerhöfer, B.; Böhm, T.; Kulyk, N.; Thiele, S.; Mayrhofer, K. J. J.; Cherevko, S. Platinum Dissolution in Realistic Fuel Cell Catalyst Layers. *Angew. Chemie - Int. Ed.* **2021**, 60 (16), 8882–8888. <https://doi.org/10.1002/anie.202014711>.
- (28) Jovanovič, P.; Petek, U.; Hodnik, N.; Ruiz-Zepeda, F.; Gatalo, M.; Šala, M.; Šelih, V. S.; Fellingner, T. P.; Gabersček, M. Importance of Non-Intrinsic Platinum Dissolution in Pt/C Composite Fuel Cell Catalysts. *Phys. Chem. Chem. Phys.* **2017**, 19 (32), 21446–21452. <https://doi.org/10.1039/C7CP03192K>.
- (29) Pavlišić, A.; Jovanovič, P.; Šelih, V. S.; Šala, M.; Hodnik, N.; Gabersček, M. Platinum Dissolution and Redeposition from Pt/C Fuel Cell Electrocatalyst at Potential Cycling. *J. Electrochem. Soc.* **2018**, 165 (6), F3161–F3165. <https://doi.org/10.1149/2.0191806jes>.
- (30) Polymeros, G.; Baldizzone, C.; Geiger, S.; Grote, J. P.; Knossalla, J.; Mezzavilla, S.; Keeley, G. P.; Cherevko, S.; Zeradjanin, A. R.; Schüth, F.; Mayrhofer, K. J. J. High Temperature Stability Study of Carbon Supported High Surface Area Catalysts—Expanding the Boundaries of Ex-Situ Diagnostics. *Electrochim. Acta* **2016**, 211, 744–753. <https://doi.org/10.1016/j.electacta.2016.06.105>.
- (31) Gatalo, M.; Bele, M.; Ruiz-Zepeda, F.; Šest, E.; Šala, M.; Kamšek, A. R.; Maselj, N.; Galun, T.; Jovanovič, P.; Hodnik, N.; Gabersček, M. A Double-Passivation Water-Based Galvanic Displacement Method for Reproducible Gram-Scale Production of High-Performance Platinum-Alloy Electrocatalysts. *Angew. Chemie - Int. Ed.* **2019**, 58 (38), 13266–13270. <https://doi.org/10.1002/anie.201903568>.
- (32) Bi, W.; Fuller, T. Temperature Effects on PEM Fuel Cells Pt/C Catalyst Degradation. *ECS Trans.* **2007**, 11 (1), 1235–1246. <https://doi.org/10.1149/1.2781037>.
- (33) Dam, V. A. T.; Jayasayee, K.; de Bruijn, F. A. Determination of the Potentiostatic Stability of PEMFC Electro Catalysts at Elevated Temperatures. *Fuel Cells* **2009**, 9

- (4), 453–462. <https://doi.org/10.1002/fuce.200800136>.
- (34) Xing, L.; Hossain, M. A.; Tian, M.; Beauchemin, D.; Adjemian, K. T.; Jerkiewicz, G. Platinum Electro-Dissolution in Acidic Media upon Potential Cycling. *Electrocatalysis* **2014**, 5 (1), 96–112. <https://doi.org/10.1007/s12678-013-0167-9>.
- (35) Inzelt, G.; Berkes, B.; Kriston, Á. Temperature Dependence of Two Types of Dissolution of Platinum in Acid Media. An Electrochemical Nanogravimetric Study. *Electrochim. Acta* **2010**, 55 (16), 4742–4749. <https://doi.org/10.1016/j.electacta.2010.03.074>.
- (36) Dam, V. A. T.; de Bruijn, F. A. The Stability of PEMFC Electrodes. *J. Electrochem. Soc.* **2007**, 154 (5), B494. <https://doi.org/10.1149/1.2714327>.
- (37) Cherevko, S.; Topalov, A. A.; Zeradjanin, A. R.; Keeley, G. P.; Mayrhofer, K. J. J. Temperature-Dependent Dissolution of Polycrystalline Platinum in Sulfuric Acid Electrolyte. *Electrocatalysis* **2014**, 5 (3), 235–240. <https://doi.org/10.1007/s12678-014-0187-0>.
- (38) Jovanovič, P.; Pavlišič, A.; Šelih, V. S.; Šala, M.; Hodnik, N.; Bele, M.; Hočevár, S.; Gabersček, M. New Insight into Platinum Dissolution from Nanoparticulate Platinum-Based Electrocatalysts Using Highly Sensitive In Situ Concentration Measurements. *Chem. Cat. Chem.* **2014**, 6 (2), 449–453. <https://doi.org/10.1002/cctc.201300936>.
- (39) Jovanovič, P.; Petek, U.; Hodnik, N.; Ruiz-Zepeda, F.; Gatalo, M.; Šala, M.; Šelih, V. S.; Fellingner, T. P.; Gabersček, M. Importance of Non-Intrinsic Platinum Dissolution in Pt/C Composite Fuel Cell Catalysts. *Phys. Chem. Chem. Phys.* **2017**, 19 (32), 21446–21452. <https://doi.org/10.1039/c7cp03192k>.
- (40) Pavlišič, A.; Jovanovič, P.; Šelih, V. S.; Šala, M.; Hodnik, N.; Hočevár, S.; Gabersček, M. The Influence of Chloride Impurities on Pt/C Fuel Cell Catalyst Corrosion. *Chem. Commun.* **2014**, 50 (28), 3732–3734. <https://doi.org/10.1039/c4cc00086b>.
- (41) Jovanovič, P.; Hodnik, N.; Ruiz-Zepeda, F.; Arcon, I.; Jozinović, B.; Zorko, M.; Bele, M.; Šala, M.; Šelih, V. S.; Hočevár, S. B.; Gabersček, M. Electrochemical Dissolution of Iridium and Iridium Oxide Particles in Acidic Media: Transmission Electron Microscopy, Electrochemical Flow Cell Coupled to Inductively Coupled Plasma Mass Spectrometry and X-Ray Absorption Spectroscopy Study. *J. Am. Chem. Soc.* **2017**, 139 (36), 12837–12846. <https://doi.org/10.1021/jacs.7b08071>.
- (42) Gatalo, M.; Hodnik, N.; Bele, M.; Jovanovič, P.; Gabersček, M.; Grom, M. Method of Treating a Platinum-Alloy Catalyst, and Device for Carrying out the Method of Treating a Platinum-Alloy Catalyst. PCT/EP2019/075855, 2019.

- (43) Meier, J. C.; Galeano, C.; Katsounaros, I.; Topalov, A. a.; Kostka, A.; Schüth, F.; Mayrhofer, K. J. J. Degradation Mechanisms of Pt/C Fuel Cell Catalysts under Simulated Start–Stop Conditions. *ACS Catal.* **2012**, *2*, 832–843. <https://doi.org/10.1021/cs300024h>.
- (44) Schlögl, K.; Mayrhofer, K. J. J.; Hanzlik, M.; Arenz, M. Identical-Location TEM Investigations of Pt/C Electrocatalyst Degradation at Elevated Temperatures. *J. Electroanal. Chem.* **2011**, *662*, 355–360. <https://doi.org/10.1016/j.jelechem.2011.09.003>.
- (45) Schulenburg, H.; Schwanitz, B.; Linse, N.; Scherer, G. G.; Wokaun, A.; Krbanjevic, J.; Grothausmann, R.; Manke, I. 3D Imaging of Catalyst Support Corrosion in Polymer Electrolyte Fuel Cells. *J. Phys. Chem. C* **2011**, *115* (29), 14236–14243. <https://doi.org/10.1021/jp203016u>.
- (46) Uchimura, M.; Sugawara, S.; Suzuki, Y.; Zhang, J.; Kocha, S. S. Electrocatalyst Durability under Simulated Automotive Drive Cycles. *ECS Transactions*. ECS 2019, pp 225–234. <https://doi.org/10.1149/1.2981858>.
- (47) Topalov, A. A.; Cherevko, S.; Zeradjanin, A. R.; Meier, J. C.; Katsounaros, I.; Mayrhofer, K. J. J. Towards a Comprehensive Understanding of Platinum Dissolution in Acidic Media. *Chem. Sci.* **2014**, *5*, 631–638. <https://doi.org/10.1039/C3SC52411F>.
- (48) Yoshida, T.; Kojima, K. Toyota MIRAI Fuel Cell Vehicle and Progress toward a Future Hydrogen Society. *Electrochem. Soc. Interface* **2015**, *24* (2), 45–49. <https://doi.org/10.1149/2.F03152if>.
- (49) Lohse-Busch, H.; Duoba, M.; Stutenberg, K.; Iliev, S.; Kern, M. *Technology Assessment of a Fuel Cell Vehicle: 2017 Toyota Mirai*; 2018.
- (50) Harzer, G. S.; Schwämmlein, J. N.; Damjanović, A. M.; Ghosh, S.; Gasteiger, H. A. Cathode Loading Impact on Voltage Cycling Induced PEMFC Degradation: A Voltage Loss Analysis. *J. Electrochem. Soc.* **2018**, *165* (6), F3118–F3131. <https://doi.org/10.1149/2.0161806jes>.
- (51) Kongkanand, A.; Ziegelbauer, J. M. Surface Platinum Electrooxidation in the Presence of Oxygen. *J. Phys. Chem. C* **2012**, *116* (5), 3684–3693. <https://doi.org/10.1021/jp211490a>.
- (52) Braaten, J.; Kongkanand, A.; Litster, S. Oxygen Transport Effects of Cobalt Cation Contamination of Ionomer Thin Films in Proton Exchange Membrane Fuel Cells. *ECS Trans.* **2017**, *80* (8), 283–290. <https://doi.org/10.1149/08008.0283ecst>.
- (53) Braaten, J. P.; Xu, X.; Cai, Y.; Kongkanand, A.; Litster, S. Contaminant Cation Effect

- on Oxygen Transport through the Ionomers of Polymer Electrolyte Membrane Fuel Cells. *J. Electrochem. Soc.* **2019**, *166* (16), F1337–F1343.
<https://doi.org/10.1149/2.0671916jes>.
- (54) Gatalo, M.; Hodnik, N.; Gabersček, M.; Bele, M. Method for Preparation of a Supported Noble Metal-Metal Alloy Composite, and the Obtained Supported Noble Metal-Metal Alloy Composite. PCT/EP2020/057334, 2020.
- (55) Ahluwalia, R. K.; Papadias, D. D.; Kariuki, N. N.; Peng, J.-K.; Wang, X.; Tsai, Y.; Graczyk, D. G.; Myers, D. J. Potential Dependence of Pt and Co Dissolution from Platinum-Cobalt Alloy PEFC Catalysts Using Time-Resolved Measurements. *J. Electrochem. Soc.* **2018**, *165* (6), 3024–3035. <https://doi.org/10.1149/2.0031806jes>.
- (56) Gatalo, M.; Ruiz-Zepeda, F.; Hodnik, N.; Dražić, G.; Bele, M.; Gabersček, M. Insights into Thermal Annealing of Highly-Active PtCu₃/C Oxygen Reduction Reaction Electrocatalyst: An in-Situ Heating Transmission Electron Microscopy Study. *Nano Energy* **2019**, *63*, 103892.
<https://doi.org/https://doi.org/10.1016/j.nanoen.2019.103892>.
- (57) Kongkanand, A.; Wagner, F. *High-Activity Dealloyed Catalysts*:
https://www.hydrogen.energy.gov/pdfs/review14/Fc087_kongkanand_2014_o.pdf
 (Date Accessed 17.3.2021).
- (58) Myers, D.; Kariuki, N.; Ahluwalia, R.; Wang, X.; Peng, J.-K. *Rationally Designed Catalyst Layers for PEMFC Performance Optimization*:
https://www.hydrogen.energy.gov/pdfs/review15/Fc106_myers_2015_o.pdf (Date Accessed 17.3.2021).
- (59) Myers, D.; Kariuki, N.; Ahluwalia, R.; Xiaohua, W.; Cetinbas, C. F.; Peng, J.-K. *Rationally Designed Catalyst Layers for PEMFC Performance Optimization*:
https://www.hydrogen.energy.gov/pdfs/review16/Fc106_myers_2016_o.pdf (Date Accessed 17.3.2021).
- (60) Mayrhofer, K. J. J.; Strmcnik, D.; Blizanac, B. B.; Stamenkovic, V.; Arenz, M.; Markovic, N. M. Measurement of Oxygen Reduction Activities via the Rotating Disc Electrode Method: From Pt Model Surfaces to Carbon-Supported High Surface Area Catalysts. *Electrochim. Acta* **2008**, *53*, 3181–3188.
<https://doi.org/http://dx.doi.org/10.1016/j.electacta.2007.11.057>.
- (61) van der Vliet, D.; Strmčnik, D.; Wang, C.; Stamenković, V. R.; Marković, N. M.; Koper, M. T. M. On the Importance of Correcting for the Uncompensated Ohmic Resistance in Model Experiments of the Oxygen Reduction Reaction. *J. Electroanal.*

- Chem.* **2010**, 647 (1), 29–34. <https://doi.org/10.1016/j.jelechem.2010.05.016>.
- (62) Gatalo, M.; Moriau, L.; Petek, U.; Ruiz-Zepeda, F.; Šala, M.; Grom, M.; Galun, T.; Jovanovič, P.; Pavlišić, A.; Bele, M.; Hodnik, N.; Gabersček, M. CO-Assisted Ex-Situ Chemical Activation of Pt-Cu/C Oxygen Reduction Reaction Electrocatalyst. *Electrochim. Acta* **2019**, 306, 377–386. <https://doi.org/10.1016/j.electacta.2019.03.153>.
- (63) Liu, T.; Wang, K.; Yuan, Q.; Shen, Z.; Wang, Y.; Zhang, Q.; Wang, X. Monodispersed Sub-5.0 Nm PtCu Nanoalloys as Enhanced Bifunctional Electrocatalysts for Oxygen Reduction Reaction and Ethanol Oxidation Reaction. *Nanoscale* **2017**, 9 (9), 2963–2968. <https://doi.org/10.1039/C7NR00193B>.
- (64) Lu, B.-A.; Sheng, T.; Tian, N.; Zhang, Z.-C.; Xiao, C.; Cao, Z.-M.; Ma, H.-B.; Zhou, Z.-Y.; Sun, S.-G. Octahedral PtCu Alloy Nanocrystals with High Performance for Oxygen Reduction Reaction and Their Enhanced Stability by Trace Au. *Nano Energy* **2017**, 33, 65–71. <https://doi.org/10.1016/j.nanoen.2017.01.003>.
- (65) Park, J.; Kanti Kabiraz, M.; Kwon, H.; Park, S.; Baik, H.; Choi, S.-I.; Lee, K. Radially Phase Segregated PtCu@PtCuNi Dendrite@Frame Nanocatalyst for the Oxygen Reduction Reaction. *ACS Nano* **2017**, 11 (11), 10844–10851. <https://doi.org/10.1021/acsnano.7b04097>.
- (66) Li, M.; Zhao, Z.; Cheng, T.; Fortunelli, A.; Chen, C.-Y.; Yu, R.; Zhang, Q.; Gu, L.; Merinov, B.; Lin, Z.; Zhu, E.; Yu, T.; Jia, Q.; Guo, J.; Zhang, L.; Goddard, W. A.; Huang, Y.; Duan, X. Ultrafine Jagged Platinum Nanowires Enable Ultrahigh Mass Activity for the Oxygen Reduction Reaction. *Science* **2016**, 354 (6318), 1414–1419.
- (67) Wang, D.; Xin, H. L.; Hovden, R.; Wang, H.; Yu, Y.; Muller, D. A.; DiSalvo, F. J.; Abruña, H. D. Structurally Ordered Intermetallic Platinum-Cobalt Core-Shell Nanoparticles with Enhanced Activity and Stability as Oxygen Reduction Electrocatalysts. *Nat. Mater.* **2013**, 12 (1), 81–87. <https://doi.org/10.1038/nmat3458>.
- (68) Moriau, L. J.; Hrnjić, A.; Pavlišić, A.; Kamšek, A. R.; Petek, U.; Ruiz-Zepeda, F.; Šala, M.; Pavko, L.; Šelih, V. S.; Bele, M.; Jovanovič, P.; Gatalo, M.; Hodnik, N. Resolving the Dilemma of Nanoparticles' Structure-Property Relationships at the Atomic Level: Case Study of Pt-Based PEM Fuel Cell Oxygen Reduction Electrocatalysts. *Cell* **2021**. <https://doi.org/10.2139/ssrn.3737808>.
- (69) Mezzavilla, S.; Baldizzone, C.; Swertz, A.-C.; Hodnik, N.; Pizzutilo, E.; Polymeros, G.; Keeley, G. P.; Knossalla, J.; Heggen, M.; Mayrhofer, K. J. J.; Schüth, F. Structure–Activity–Stability Relationships for Space-Confined Pt_xNi_y Nanoparticles in the Oxygen Reduction Reaction. *ACS Catal.* **2016**, 6 (12), 8058–8068.

<https://doi.org/10.1021/acscatal.6b02221>.

- (70) Gatalo, M.; Jovanovič, P.; Polymeros, G.; Grote, J.-P.; Pavlišič, A.; Ruiz- Zepeda, F.; Šelih, V. S.; Šala, M.; Hočevan, S.; Bele, M.; Mayrhofer, K. J. J.; Hodnik, N.; Gabersček, M. Positive Effect of Surface Doping with Au on the Stability of Pt-Based Electrocatalysts. *ACS Catal.* **2016**, 6 (3). <https://doi.org/10.1021/acscatal.5b02883>.